Synthesis, characterization and size control of zerovalent iron nanoparticles anchored on montmorillonite

FAN MingDe[1, 2], YUAN Peng[1*], CHEN TianHu[3], HE HongPing[1], YUAN AiHua[4], CHEN KangMin[5], ZHU JianXi[1] & LIU Dong[1,6]

[1] *Guangzhou Institute of Geochemistry, Chinese Academy of Sciences, Guangzhou 510640, China;*

[2] *College of Environment and Resources, Inner Mongolia University, Hohhot 010021, China;*

[3] *School of Resources and Environmental Engineering, Hefei University of Technology, Hefei 230009, China;*

[4] *School of Materials Science and Engineering, Jiangsu University of Science and Technology, Zhenjiang 212003, China;*

[5] *School of Materials Science an Engineering, Jiangsu University, Zhenjian 212003, China;*

[6] *Graduate School of the Chinese Academy of Sciences, Beijing 100039, China*

Zerovalent iron nanoparticles have been successfully synthesized using sodium borohydride solution reduction of ferric trichloride hexahydrate in the presence of montmorillonite as an effective protective reagent and support as well. A combination of characterizations reveals that with high monodispersity these obtained iron nanoparticles are well dispersed on clay surface, virginal from boron related impurity, and oxidation resistant well with iron core-iron oxide shell structure. The shell thickness of 3 nm remains almost invariable under ambient conditions. The size control of these iron nanoparticles has been achieved by tailoring the amount of the ferric iron, which mainly depends on the protective action of montmorillonite.

zerovalent iron nanoparticles, montmorillonite, core-shell structured, chemical solution reduction

Much attention in the past years has been paid to zerovalent iron nanoparticles (ZVINs) for their prominent magnetic properties and great potential in a variety of applications including ferrofluids [1], magnetic resonance imaging contrast agents [2], magnetic recording media [3], heterogenous catalysts [4], and environmental remediation [5−7]. Different methods have been so far developed for the synthesis of ZVINs, among them chemical reduction of ferric iron (Fe(III)) or ferrous iron (Fe(II)) in solution with borohydride (e.g. $NaBH_4$ or KBH_4) has a key advantage of simplicity and can be done in most chemistry labs with simple reagents [8]. Nevertheless, this method suffers a disadvantage that the iron product strongly depends on the preparation conditions. Almost any changes in the preparation process might have obvious influences on the resultant iron [9]. In addition, as some studies revealed [10,11] this

method is prone to introduce boron impurity into the crystal lattice of iron. Also, this method is limited by ease to oxidize and addiction to aggregate of ZVINs.

A crucial problem in obtaining ZVINs is that their high surface energy and reactivity make them easy to oxidize and inconvenient for practical applications. One approach for controlling the oxidation is to coat the particles, creating a core-shell structure. The shell can be composed of different materials, among them the native iron oxide is attractive and intensively studied for its almost unavoidable formation and good performance to control the oxidation of iron core [12−15]. The aggregation of ZVINs, mainly derived from the behavior to decrease their surface free energy can be, to a great extent, inhibited by dispersing them with organic or inorganic protective reagents such as polymers [16], surfactants [17], dendrimers [18], resins [19], aluminas [20], active carbons [21], zeolites [22], and clay minerals [23]. Compared with other protective reagents, inorganic chemically inert clay

*Corresponding author (email: yuanpeng@gig.ac.cn)

minerals are more cost-effective and environment-friendly, and they are also commonly used as supports for nanoparticles. Stabilizing nanoparticles on supports can enhance the stability of nanoparticles for pelletization, storage, and transportation [24], as well as can favor the reuse and recycling of nanoparticles from reaction mixture [25,26]. Of such clay minerals, montmorillonite (Mt) is often used as an effective protective reagent and support as well. Mt is a naturally occurring 2:1 type layered alumonosilicate with turbostratic structure, in which each layer comprises an alumina octahedral sheet sandwiched between two silica tetrahedral sheets, and the layer has a permanent negative charge resulting from isomorphous substitution occurring mainly in the octahedral sheet. Such layers are stacked by weak dipolar or Van der Waals forces, leading to the intercalation of charge compensating cations into the interlayer space and causing Mt to be easily expanded along the *c* direction [27]. With Mt as protective reagent and support many metallic nanoparticles such as Rh [25], Pt [23], and Au [28] have been synthesized through borohydride reduction of the corresponding precursor salts. However, maybe due to the complications of the borohydride method itself, few studies as we know are available related to the synthesis of ZVINs using borohydride reduction in the presence of Mt. For example, in the study about sodium borohydride solution reduction of Fe^{2+}-exchanged Mt, only Fe-B amorphous clusters were obtained [10]. In this sense, it would be very interesting to synthesize Mt supported ZVINs and to explore the effect of Mt on the related characteristics and formation mechanism of the iron nanoparticles.

In this paper, we present our results obtained from synthesizing ZVINs well dispersed on Mt using sodium borohydride reduction of Fe(III) in solution. The action and related mechanism of Mt as protective reagent and support are intensively explored. Considering that the intrinsic properties of a metal nanoparticle can be largely affected by its size [29], size control of the Mt supported ZVINs is also attempted by tailoring the amount of the Fe(III) used.

1 Materials and methods

1.1 Materials

Raw Mt sample from Inner Mongolia, China was purified and classified by the conventional sedimentation method [30], and the fraction less than 2 μm was collected. The Mt fine fraction was then ion-exchanged with NaCl solution according to the literature method [31] to obtain Na^+-montmorillonite (Na^+-Mt). The cationic exchange capacity (CEC) of thus obtained Na^+-Mt was determined according to the ammonium acetate saturation method [32] and was found to be 111.1 mmol/100 g. The Na^+-Mt was used as protective reagent and support for the synthesis of ZVINs. $FeCl_3 \cdot 6H_2O$ and $NaBH_4$ available locally were all of analytical grade and used as received. Distilled water was used throughout this work.

1.2 Preparation of montmorillonite supported zerovalent iron nanoparticles

Mt supported ZVINs were synthesized using sodium borohydride solution reduction of $FeCl_3 \cdot 6H_2O$ according to the method reported by Wang and Zhang [5] with some modifications, where the Mt was used as protective reagent and support and the amount of the Fe(III) was tailored to control the size of the supported ZVINs. In a typical procedure, Na^+-Mt (2.0 g) was stirred in 100 mL water for 24 h, and then $FeCl_3 \cdot 6H_2O$ (corresponding to 1, 2, 4, 6 times CEC of Na^+-Mt) was added to the aqueous clay suspension. The mixture was stirred for another 24 h and then 100 mL freshly prepared $NaBH_4$ solution was dropwise added under stirring. The molar ratio of boron to iron was 4:1. After $NaBH_4$ was added the solution turned to black, indicating the reduction of ferric iron. All the experiments were carried out at room temperature and no precautions were taken to eliminate oxygen from the reaction vessel. After several centrifugation/redispersion cycles in 50% v/v aqueous ethanol solution then in acetone, the final product was vacuum dried at 60°C for 24 h. The final product prepared at a Fe(III) amount of 1 CEC of clay was labeled as MtZVI-1 and the others were labeled in a similar fashion. Except the absence of clay, pure ZVINs were prepared with the same procedure for MtZVI-6 to ensure the sufficient product amount. This pure product was labeled as ZVI-P.

1.3 Characterization methods

Crystal phases were identified by X-ray diffraction (XRD) with a Bruker D8 Advance diffractometer using Cu*Kα* radiation ($\lambda = 0.154$ nm). All samples were recorded at a continuous scanning speed of 4° (2θ)/min with a fixed power source of 40 kV and 30 mA. The mean diameter, *D*, of the crystallites of the particles was estimated from the pure X-ray diffraction broadening, β, by the Scherrer formula: $D = k\lambda/\beta\cos\theta$, where *k* is a constant approximately equal to unity and related both to the crystallite shape and to the way in which β and *D* are defined; λ and θ are the radiation wave-length and Bragg angle, respectively.

Microstructure characterization and particle size determination were carried out by a combination of a 100 kV JEOL JEM-100CXII transmission electron microscope (TEM) attached to an electron diffractometer, a 200 kV JEOL JEM- 2100 high resolution transmission electron microscope (HRTEM), and a 5 kV FEI-Sirion 200 field emission scanning electron microscope (FESEM) attached to an Oxford INCA energy dispersive X-ray spectroscopy (EDX).

The sample for TEM or HRTEM was prepared by sonication of the powders in ethanol. Then, a holey carbon-coated copper grid was dipped in the suspension and then allowed to air-dry. The sample for FESEM was prepared by dispersing the powders in ethanol and then evaporation of a drop of the suspension on a copper conductive tape. The
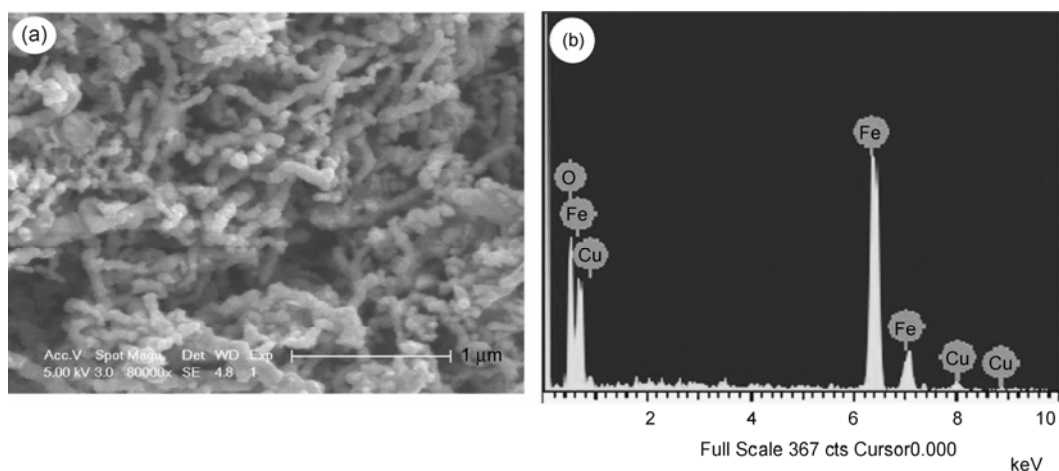
Figure 1 (a) FESEM image and (b) corresponding EDX spectrum of ZVI-P.

sputtering of the sample with gold in this procedure was not adopted for avoiding the confusion between the iron and possible gold particles.

2 Results and discussion

2.1 Pure zerovalent iron nanoparticles

As shown in Figure 1(a), the pure zerovalent iron nanoparticles (ZVI-P) synthesized in homogeneous solution without Mt are roughly spherical and connected in chains of about 80 nm in width. This chain-like morphology is caused by magnetostatic attraction between the iron particles. Similar observations are also reported in literature [33,34]. The intense peaks of α-Fe accompanied with the weak peaks of iron oxide in the XRD Pattern (Figure 2(a)) indicate the existence of a core-shell structure of the pure iron, where the core consists of metallic α-Fe whereas the shell is composed of iron oxide. The iron oxide might be magnetite and/or maghemite. Due to similar lattice constants, the two oxides are not easily distinguished by XRD. Exact identification of the two phases by Mössbauer spectroscopy is being conducted.

In the EDX spectrum of ZVI-P (Figure 1(b)) no boron is detected, which might be due to the trace amount or the separating state of the element. Based on the XRD pattern of ZVI-P (Figure 2(a)), the lattice constant of the pure iron *a* = 2.866 Å, refined by least square fit following the TREOR algorithm, shows negligible variation to the reported value of body-centered cubic α-Fe (JCPDS No. 06-0696). This coincidence prefers that the boron segregates in a separating state from the pure iron. As mentioned above, some researchers have revealed that the borohydride method could introduce boron impurity into the crystal lattice of iron [10]. The difference between this study and the one of Zhang and Manthiram [10] might be attributed to the different experimental parameters adopted respectively. Particularly, we adopted the boron to iron molar ratio of 4:1 as recom-

mended by Wang and Zhang [5], where the ratio is suitable for the synthesis of ZVINs. Compared with the molar ratio of about 12:1 adopted by Zhang and Manthiram [10], the decrease of the ratio to 4:1 indicates that less borohydride was used in this study, which might reduce the chance of boron incorporating into the iron crystal lattice. The iron and oxygen signals in the EDX spectrum are from the resultant iron nanoparticles, and the copper signals from the copper conductive tape (Figure 1(b)).
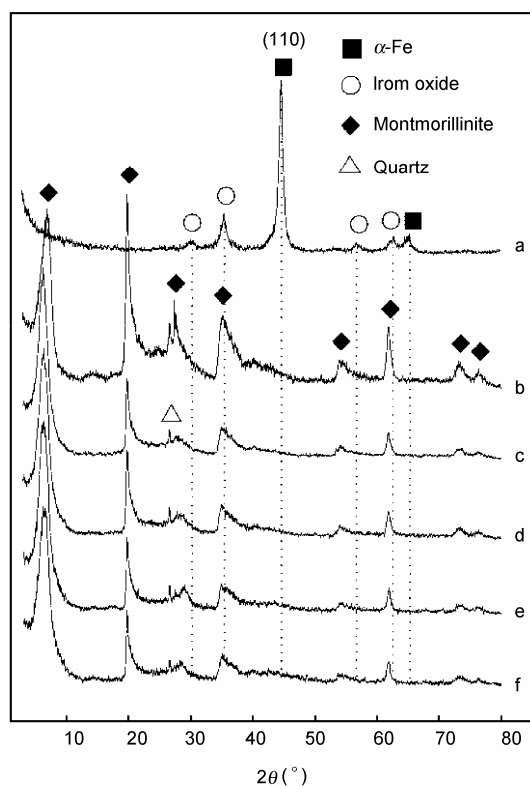

Figure 2 XRD patterns of (a) ZVI-P, (b) Na⁺-Mt, (c) MtZVI-1, (d) MtZVI-2, (e) MtZVI-4, and (f) MtZVI-6.
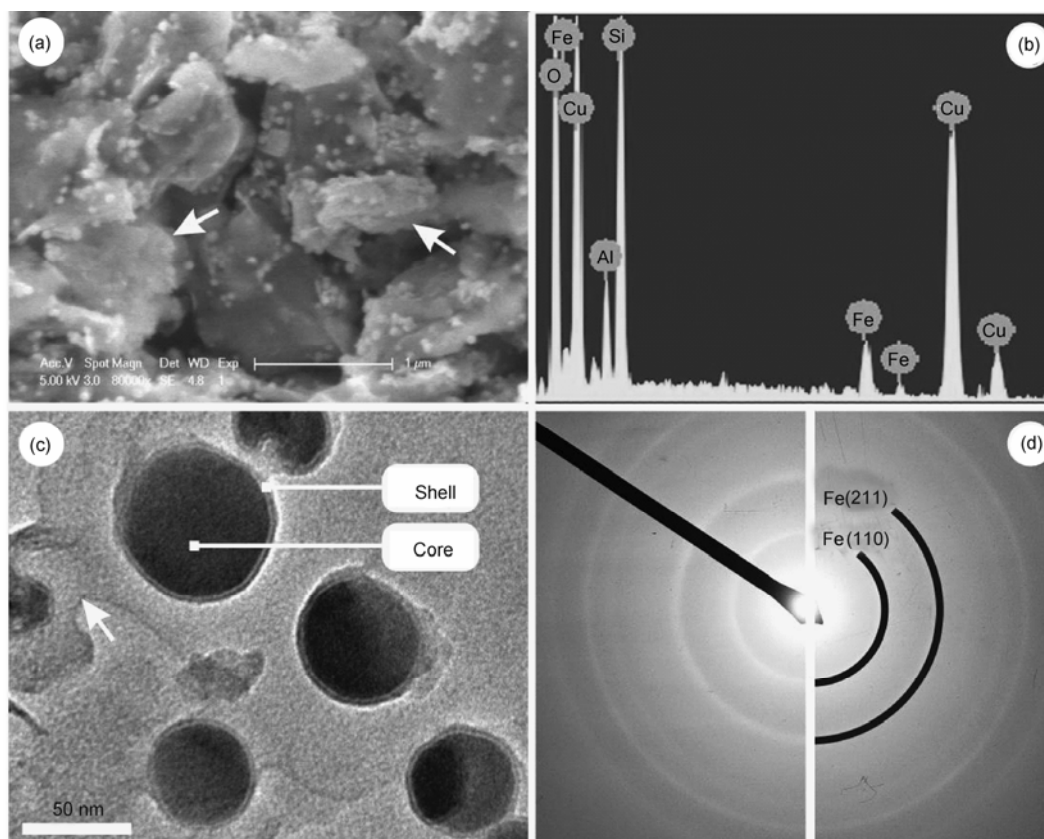
Figure 3   (a) FESEM image, (b) corresponding EDX spectrum, (c) high magnification TEM image, and (d) corresponding SAED pattern of MtZVI-6. White arrows indicate montmorillonite particles.

2.2   Montmorillonite supported zerovalent iron nanoparticles

For the purpose of comparison with ZVI-P, MtZVI-6 is selected as a typical sample and explored in detail. Figure 3 and Figure 5(d) show the microscopy overview of MtZVI-6. The roughly spherical iron nanoparticles are well dispersed on clay surface as shown in both the FESEM and low magnification TEM images (Figure 3(a) and the left panel of Figure 5(d)). The particle size distribution fitted with normal function (the right panel of Figure 5(d)) is obtained by sampling a minimum of 300 particles from the TEM images of the sample, which gives a mean particle size and relative standard deviation (RSD) of 55 nm and 0.2, respectively. The small RSD value implies a narrow size distribution and high monodispersity of the iron particles. Similar to Na^+-Mt (Figure 2(b)), only the peaks of Mt can be found in the XRD pattern for MtZVI-6 (also for MtZVI-1, 2, 4) (Figure 2(c)–(f)). In the XRD pattern of MtZVI-6, no iron related peaks can be distinguished due to the fact that the fine crystalline size of the supported iron makes its peaks merged into the background corresponding to Scherrer effect. Based on this effect the crystalline size of the supported iron is less than 4 nm. However, determined from the intense (110) reflection of the pure iron (Figure 2(a)), the crystalline size of the pure iron is about 10 nm using Scherrer formula.

Compared with the pure iron, both the crystalline size and the particle size of the supported iron are reduced, and the aggregation of the supported iron is largely inhibited, which is related to the action of Mt used as an effective protective reagent and support as well. The Mt particles dispersed in solution favor heterogeneous nucleation, according to which the clay can control the nucleation and prevent the mutual contact of the iron clusters. Similar action was also reported for Laponite used in forming gold and silver nanoparticles [35]. It is noteworthy that some short chains and small aggregations also exist in MtZVI-6 (the left panel of Figure 5(d)), which might result from the heterogeneous surface activities of the clay used.

The continuously diffuse diffraction rings appeared in the selected area electron diffraction (SAED) pattern of MtZVI-6 (Figure 3(d)) reveal the polycrystalline nature of the supported iron nanoparticles composed of fine random oriented crystal grains. The observed two rings assigned to the (110) and (211) plans of α-Fe combined with the iron and oxygen signals in the EDX spectrum of this sample (Figure 3(b)) imply an iron core-iron oxide shell structure of the particles, as the pure iron nanoparticles. The iron signals are derived from the α-Fe core and the iron oxide shell, whereas the oxygen signal is exclusively derived from the iron oxide shell. In addition, the silicon and aluminum signals are derived from the clay used (Figure 3(b)). Notably,
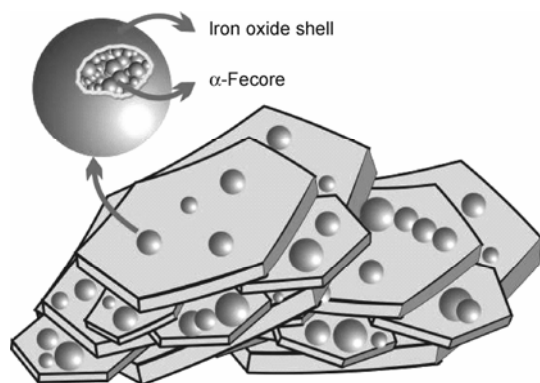
Figure 4 Schematic representation of structure characteristics of montmorillonite supported iron nanoparticles with polycrystalline α-Fe core-iron oxide shell structure.

similar to the pure iron boron signal is absent in the EDX spectrum of MtZVI-6, excluding the possibility of introducing boron into the crystal lattice of the supported iron.

As revealed by Shafranovsky and Petrov [14], fast oxidation of nascent iron powder is likely to form a mixture of magnetite and maghemite. No precautions were taken to eliminate oxygen from the reaction vessel in this study, which is likely to cause nascent iron to be fast oxidized and facilitated the formation of iron oxide shell. This formation can be well supported by the EDX analysis of MtZVI-6. Furthermore, the high magnification TEM image of MtZVI-6 (Figure 3(c)) clearly shows the iron oxide shells on the iron cores, where the iron oxide shells are brighter than the iron cores resulting from their different mass-thickness contrasts. It is worthy to note that the iron oxide shells have an almost invariable thickness of 3 nm independent of the particle size, which can be explained by the Caberra-Mott theory as some studies referred [12,14,15]. According to this theory, upon the initial attachment of oxygen onto the surface of iron and the formation of a thin oxide layer, the electron tunnels through the thin oxide layer and ionizes the oxygen, leading to an electrical field between the iron and the surface of the oxide layer. The electrical field will then drive the outward diffusion of the ionized iron. At room temperature, about 0.2 fs are needed to form an initial 1-nm-thick oxide layer on a freshly exposed iron surface, and 40 s for 2 nm, 40 weeks for 3 nm, 600 years for 4 nm [15,36]. Considering that MtZVI-6 is obtained at room temperature and the period of time till its microscopy imaging is less than 40 weeks, the iron oxide shells are reasonably kept at 3 nm corresponding to the Caberra-Mott theory. Furthermore, the long period of 600 years for the thickening of the shell to 4 nm makes the iron oxidation resistant well at ambient conditions. Taking the above arguments into consideration, the structure characteristics of the clay supported iron nanoparticles can be illustrated by the schematic representation shown in Figure 4.

2.3 Size control of montmorillonite supported zerovalent iron nanoparticles by tailoring the amount of Fe(III)

Figures 5(a)–(d) show the TEM images and the corresponding size distributions of MtZVI-1, 2, 4, 6. The size distributions are fitted with normal functions. For these samples, the iron particles are all well dispersed on clay surface with high monodispersity indicated by their small RSD values.

The average particle sizes of MtZVI-1 and 2 are 30 and 34 nm, respectively (Figures 5(a) and (b)). With increasing the amount of Fe(III), the sizes of MtZVI-3 and 4 increase to 58 and 55 nm, respectively (Figures 5(c) and (d)). This statistical increase of the particle size with the amount of Fe(III) can be attributed to the action of Mt as an effective protective reagent. Since the negatively charged sites on the surface of basal plane of Mt can act as adsorption sites for cations as well as protective ones, Fe(III) can adsorb on the basal plane of Mt particles by electrostatic interaction. By adding sodium borohydride, the nucleation would start at two sites: one is Fe(III) adsorbed on the basal plane and the other is free Fe(III) in bulk solution. Small particles would be formed from the adsorbed Fe(III) due to the limitation of Mt particles to their nucleation and growth, whereas large particles would be formed from the free Fe(III) due to their almost unlimited nucleation and growth. If the amount of Fe(III) is quite large, the protective action of Mt is less effective so that more Fe(III) would exist in free state and then more particles of large size would be formed in bulk solution. These large particles, to decrease their surface free energy, would then adhere to the clay surface with great possibility, which would result in large average particle size. In this study, since the amount of Mt is fixed, increasing the amount of Fe(III) would make the protective action of Mt less effective and form large particles. Aihara et al. [35] provided similar explanations for the size control of gold or silver nanoparticles by the variation of Laponite amount. It is worth noting that only in a certain range the amount of Fe(III) would obviously affect the particle size. For example, the average particle sizes of MtZVI-1 and 2 are similar (Figures 5(a) and (b)), the same case also occurs for MtZVI-4 and 6 (Figures 5(c) and (d)). However, the particle size dramatically increases from 34 nm for MtZVI-2 to 58 nm for MtZVI-4 (Figures 5(b) and (c)). This phenomenon is, to a great degree, related to the negative charges of Mt, which play an important role in the size control as discussed above. Limited amounts of these charges are available on Mt. Thus, for a fixed Fe(III) amount Mt would affect the particle size in a certain amount range. Rationally, when the amount of Mt is fixed the Fe(III) would also affect the particle size in a certain amount range.

The cationic exchange capacity (CEC) of Mt corresponds to the number of its negative charges, which make clay have the propensity for adsorbing cationic species from solution [30]. When the amount of Fe(III) is below the CEC, the protective action of Mt is effective so that small particles
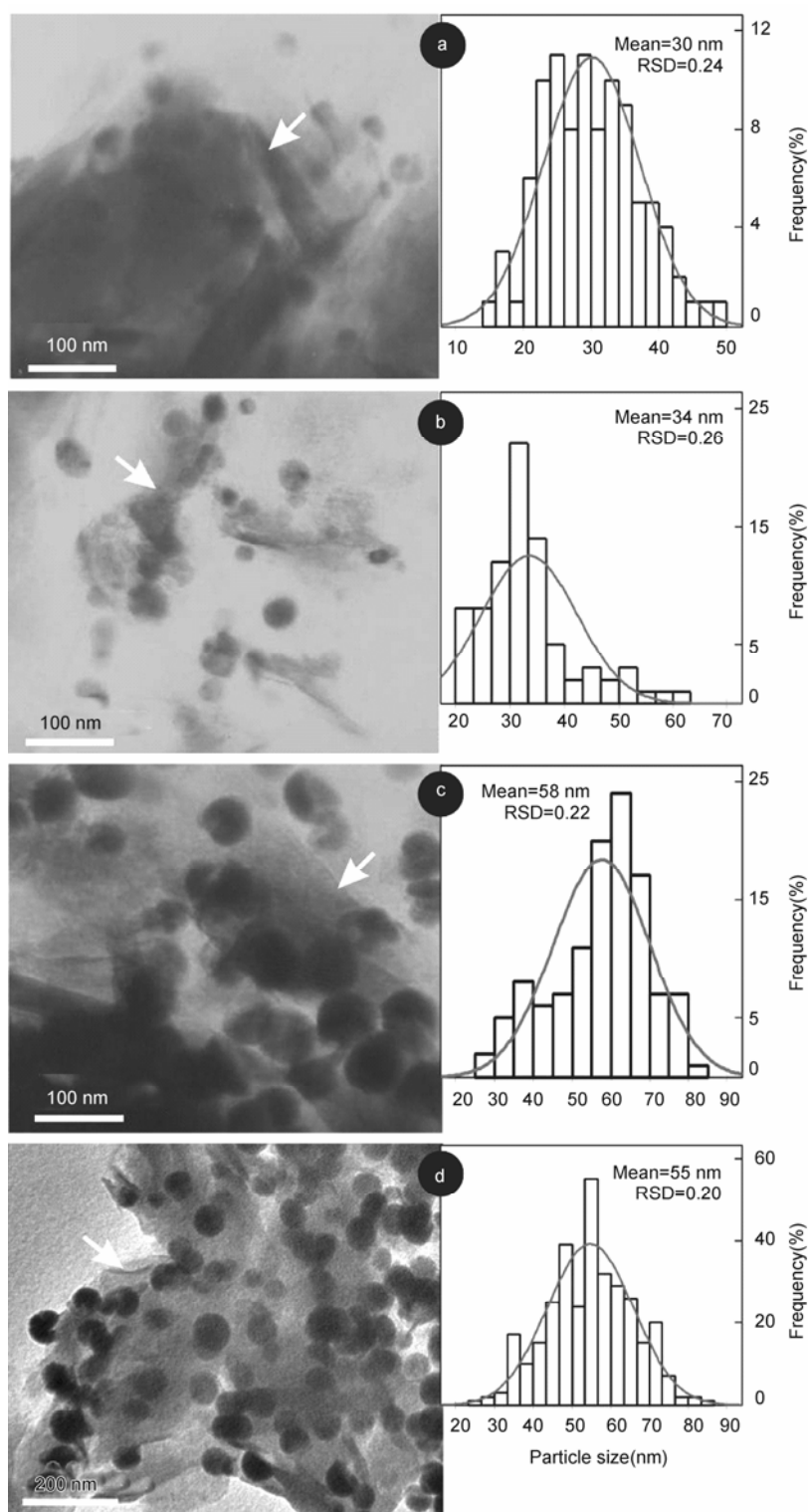
Figure 5   TEM images (in left panels) and corresponding size distributions (in right panels) of (a) MtZVI-1, (b) MtZVI-2, (c) MtZVI-4, and (d) MtZVI-6. Size distributions are fitted with normal functions, and white arrows indicate montmorillonite particles.

would be formed; when the amount of Fe(III) is above the CEC, the protective action of Mt is less effective so that large particles would be formed. However, similar average particle sizes are obtained in this study when the Fe(III)

amounts are 1 and 2 times the Mt CEC, which might be due to the fact that the protective action of Mt is not absolutely derived from its negative charges, other contributions would also exist. Consequently, when the amount of Fe(III) ex-

ceeds the CEC, the protective action of Mt can also be effective. Some studies have shed some light on the possible contributions different from the negative charges of clay. Aihara et al. [35] suggested that to reduce their surface free energy the behavior of nanoparticles to adhere on clay surface would have contribution to the protective action of clay. Similar result was also suggested by Király et al. [37] in their study about ultrafine palladium particles on clays. Our study seemed to offer another support for this suggestion. Nevertheless, deep insights on the contributions to the protective action of Mt are also needed.

3   Conclusions

Montmorillonite supported zerovalent iron nanoparticles have been successfully synthesized using sodium borohydride chemical reduction of Fe(III) in solution. The aggregation of these obtained iron particles are largely inhibited by montmorillonite used as an effective protective reagent and support as well. With high monodispersity these iron particles are virginal from boron related impurity, well dispersed on clay surface, and oxidation resistant well with polycrystalline iron core-iron oxide shell structure. The shell thickness remains almost invariable at 3 nm, which protects the iron core from further oxidation. The supporting treatment can have an influence on favoring the reuse and recycling of these iron particles and making these iron particles of great potential in practical applications.

The size control of these iron particles has been achieved by tailoring the amount of the Fe(III) used. For a fixed montmorillonite amount, the average size of these iron particles increases with the amount of the Fe(III), and the Fe(III) affects the particle size in a certain amount range. This size control mainly depends on the protective action of montmorillonite.

1   López-López M T, Gómez-Ramírez A, Durán J D G, et al. Preparation and characterization of iron-based magnetorheological fluids stabilized by addition of oganoclay prticles. Langmuir, 2008, 24: 7076–7084

2   Stuckey D J, Carr C A, Martin-Rendon E, et al. Iron particles for noninvasive monitoring of bone marrow stromal cell engraftment into, and isolation of viable engrafted donor cells from, the heart. Stem Cells, 2006, 24: 1968–1975

3   Hayashi K, Ohsugi M, Kamigaki M, et al. Functional effects of carbon-coated iron metal particles for magnetic recording media. Electrochem Solid-State Lett, 2002, 5: J9–J12

4   Guczia L, Steflerb G, Gesztia O, et al. CO hydrogenation over cobalt and iron catalysts supported over multiwall carbon nanotubes: Effect of preparation. J Catal, 2006, 244: 24–32

5   Wang C B, Zhang W X. Synthesizing nanoscale iron particles for rapid and complete dechlorination of TCE and PCBs. Environ Sci Technol, 1997, 31: 2154–2156

6   Ponder S M, Darab J G, Mallouk T E, et al. Remediation of Cr(VI) and Pb(II) aqueous solutions using supported, nanoscale zero-valent iron. Environ Sci Technol, 2000, 34: 2564–2569

7   Wilkin R, McNeil M S. Laboratory evaluation of zero-valent iron to treat water impacted by acid mine drainage. Chemosphere, 2003, 53: 715–725

8   Sun Y P, Li X Q, Cao J, et al. Characterization of zero-valent iron nanoparticles. Adv Colloid Interface Sci, 2006, 120: 47–56

9   Rodrigues A R, Soares J M, Machado F L A, et al. Synthesis of α-Fe particles using a modified metal-membrane incorporation technique. J Magn Magn Mater, 2007, 310: 2497–2499

10   Zhang L, Manthiram A. Ambient temperature synthesis of fine metal particles in montmorillonite clay and their magnetic properties. Nanostruct Mater, 1996, 7: 437–451

11   Balakrishnan S, Bonder M J, Hadjipanayis G C. Particle size effect on phase and magnetic properties of polymer-coated magnetic nanoparticles. J Magn Magn Mater, 2009, 321: 117–122

12   Kuhn L T, Bojesen A, Timmermann L, et al. Structural and magnetic properties of core-shell iron-iron oxide nanoparticles. J Phys Condes Matter, 2002, 14: 13551–13567

13   Carpenter E E, Calvin S, Stroud R M, et al. Passivated iron as core-shell nanoparticles. Chem Mater, 2003, 15: 3245–3246

14   Shafranovsky E A, Petrov Yu I. Aerosol Fe nanoparticles with the passivating oxide shell. J Nanopart Res, 2004, 6: 71–90

15   Wang C M, Baer D R, Thomas L E, et al. Void formation during early stages of passivation: Initial oxidation of iron nanoparticles at room temperature. J Appl Phys, 2005, 98: 094308–094307

16   Mahajan D, Desai A, Rafailovich M, et al. Synthesis and characterization of nanosized metals embedded in polystyrene matrix. Composites Part B, 2006, 37: 74–80

17   Pal T, Sau T K, Jana N R. Reversible formation and dissolution of silver nanoparticles in aqueous surfactant media. Langmuir, 1997, 13: 1481–1485

18   Niu Y, Crooks R M. Dendrimer-encapsulated metal nanoparticles and their applications to catalysis. C R Chimie, 2003, 6: 1049–1059

19   Najman R, Cho J K, Coffey A F, et al. Entangled palladium nanoparticles in resin plugs. Chem Commun, 2007, 47: 5031–5033

20   Calla J T, Davis R J. Investigation of alumina-supported Au catalyst for CO oxidation by isotopic transient analysis and X-ray absorption spectroscopy. J Phys Chem B, 2005, 109: 2307–2314

21   Carrettin S, McMorn P, Johnston P, et al. Selective oxidation of glycerol to glyceric acid using a gold catalyst in aqueous sodium hydroxide. Chem Commun, 2002, 7: 696–697

22   Moreno M S, Weyland M, Midgley P A, et al. Highly anisotropic distribution of iron nanoparticles within MCM-41 mesoporous silica. Micron, 2006, 37: 52–56

23   Manikandan D, Divakar D, Sivakumar T. Utilization of clay minerals for developing Pt nanoparticles and their catalytic activity in the selective hydrogenation of cinnamaldehyde. Catal Commun, 2007, 8: 1781–1786

24   Yuan P, Fan M D, Yang D, et al. Montmorillonite-supported magnetite nanoparticles for the removal of hexavalent chromium [Cr(VI)] from aqueous solutions. J Hazard Mater, 2009, 166: 821–829

25   Papp S, Szel J, Oszko A, et al. Synthesis of polymer-stabilized nanosized rhodium particles in the interlayer space of layered silicates. Chem Mater, 2004, 16: 1674–1685

26   Király Z, Dékány I, Mastalir Á, et al. In situ generation of palladium nanoparticles in smectite clays. J Catal, 1996, 161: 401–408

27   Pinnavaia T J. Intercalated clay catalysts. Science, 1983, 220: 365–371

28 Paek S M, Jang J U, Hwang S J, et al. Exfoliation-restacking route to Au nanoparticle-clay nanohybrids. J Phys Chem Solids, 2006, 67: 1020–1023

29 Sun Y, Xia Y. Shape-controlled synthesis of gold and silver nanoparticles. Science, 2002, 298: 2176–2179

30 Bergaya F, Theng B K J, Lagaly G. Handbook of Olay Science. Amsterdam/London: Elsevier, 2006

31 Chen B, Evans J R G. Preferential intercalation in polymer-clay nanocomposites. J Phys Chem B, 2004, 108: 14986–14990

32 Mackenzie R C. A micromethod for determination of CEC of clay. J Colloid Sci, 1951, 6, 219–222

33 Huang K C, Ehrman S H. Synthesis of iron nanoparticles via chemical reduction with palladium ion seeds. Langmuir, 2007, 23: 1419

–1426

34 Huang K C, Chou K S. Microstructure changes to iron nanoparticles during discharge/charge cycles. Electrochem Commun, 2007, 9: 1907–1912

35 Aihara N, Torigoe K, Esumi K. Preparation and characterization of gold and silver nanoparticles in layered Laponite suspensions. Langmuir, 1998, 14: 4945–4949

36 Fung K K, Qin B X, Zhang X X. Passivation of α-Fe nanoparticle by epitaxial γ-Fe_2O_3 shell. Mater Sci Eng A, 2000, 286: 135–138

37 Király Z, Veisz B, Mastalir Á, et al. Preparation of ultrafine palladium particles on cationic and anionic clays, mediated by oppositely charged surfactants: Catalytic probes in hydrogenations. Langmuir, 2001, 17: 5381–5387